https://doi.org/10.5194/cp-2019-58
Preprint. Discussion started: 13 June 2019

Climate of the Past Discussions
Open Access

Hypersensitivity of glacial temperatures in Siberia

Pepijn Bakker[1,2], Irina Rogozhina[2,3,4], Ute Merkel[2], and Matthias Prange[2]

[1]Department of Earth Sciences, Vrije Universiteit Amsterdam, Amsterdam, The Netherlands
[2]MARUM-Center for Marine Environmental Sciences, University of Bremen, Bremen, Germany
[3]Norwegian University of Science and Technology, Trondheim, Norway
[4]Institute of Physics of the Earth, Russian Academy of Science, Russia

Correspondence: Pepijn Bakker (p.bakker@vu.nl)

Abstract. Climate change in Siberia is currently receiving a lot of attention as large permafrost-covered areas could provide a strong positive feedback to global warming through the release of carbon that has been sequestered there on glacial-interglacial time scales. Geological evidence and climate model experiments show that the Siberian region also played an exceptional role during glacial periods. The region that is currently known for its harsh cold climate did not experience major glaciations during the last ice age, including its severest stages around the Last Glacial Maximum (LGM). On the contrary, it is thought that glacial summer temperatures were comparable to present-day.

We combine LGM experiments from the second and third phases of the Paleoclimate Modelling Intercomparison Project (PMIP2 and PMIP3) with sensitivity experiments with the Community Earth System Model (CESM). Together these climate model experiments reveal that the intermodel spread in LGM summer temperatures in Siberia is much larger than in any other region of the globe and suggest that temperatures in Siberia are highly susceptible to changes in the imposed glacial boundary conditions, the included feedbacks and processes, and to the model physics of the different components of the climate model. We find that changes in the large-scale atmospheric stationary wave pattern and associated northward heat transport drive strong local snow and vegetation feedbacks and that this combination explains the susceptibility of LGM summer temperatures in Siberia. This suggests that a small difference between two glacial periods in terms of climate, ice buildup or their respective evolution towards maximum glacial conditions, can lead to strongly divergent summer temperatures in Siberia, that are sufficiently strong to allow for the buildup of an ice sheet during some glacial periods, while during others, above-freezing summer temperatures will preclude a multi-year snow-pack from forming.

1 Introduction

During the Last Glacial Maximum (LGM; ~24-18 ka ago) ice sheets covered large parts of the Northern Hemisphere continents. Over North America and northwestern Eurasia continental ice sheets extended from the Arctic ocean down to ~50°N. The most notable exception was northeastern Siberia, a region that remained largely ice-free during the LGM according to archaeological evidence (Pitulko et al., 2004), geological reconstructions and permafrost records (Boucsein et al., 2002; Schirrmeister, 2002; Hubberten et al., 2004; Gualtieri et al., 2005; Stauch and Gualtieri, 2008; Wetterich et al., 2011; Jakobsson et al., 2014; Ehlers et al., 2018), and combined model-data driven ice-sheet reconstructions (Abe-Ouchi et al., 2013; Kleman et al., 2013; Peltier

https://doi.org/10.5194/cp-2019-58
Preprint. Discussion started: 13 June 2019

et al., 2015). This is intriguing given the fact that the area presently extends as far north as ~75°N, and extended even further north during the LGM when a large part of the Siberian continental shelf was exposed because of sea-level lowering.

Reconstructing Quaternary ice sheet limits and assigning geological ages has proven a difficult task for the Siberian region for various reasons (e.g., Jakobsson et al., 2014). Svendsen et al. (2004) synthesized all existing geological data and concluded that since the last interglacial period (~130-115 ka ago), most of Siberia has remained ice-free, with the exception of the high-altitude Putorana Plateau and the coastal areas of the Kara Sea. Independent evidence from permafrost records (Boucsein et al., 2002; Schirrmeister, 2002; Hubberten et al., 2004; Wetterich et al., 2011), marine sediment cores (Darby et al., 2006; Polyak et al., 2004, 2007, 2009; Adler et al., 2009; Backman et al., 2009) and dating of mollusc shells (Basilyan et al., 2010) also indicates that the entire region between the Taymyr Peninsula and the Chukchi Sea remained ice free and was covered by tundra-steppe during the LGM and that the last grounded ice impacts in different sectors of this region are dating back to MIS 6, or potentially MIS 5 within the dating uncertainties (Stauch and Gualtieri, 2008). Hence, the existing geological evidence indicates that ice sheets covered large parts of western Siberia (Svendsen et al., 2004; Patton et al., 2015; Ehlers et al., 2018) and the East Siberian continental shelf (Niessen et al., 2013; Jakobsson et al., 2014, 2016) prior to the last glacial period but it remains unclear how often northeastern Siberia experienced large-scale glaciations during the different glacial periods of the Quaternary. Nonetheless, it appears that this far northern region was covered by ice during some glacial periods, while it remained ice free during others.

A number of studies have simulated the East Siberian LGM climate and ice sheet growth (e.g. Krinner et al., 2006; Charbit et al., 2007; Ganopolski et al., 2010; Abe-Ouchi et al., 2013; Beghin et al., 2014; Peltier et al., 2015; Liakka et al., 2016). They show widely different results, from ice-free conditions to the buildup of a large ice sheet covering most of Siberia, and therefore the correspondence with proxy-based reconstructions ranges from good to very poor.

Over the years, a number of possible mechanisms have been suggested to explain the lack of an ice sheet covering eastern Siberia during the LGM, and perhaps therewith also explain the divergent results of coupled climate-ice-sheet simulations for this region during the LGM. The most widely discussed mechanisms involve changes in atmospheric dust load, orographic precipitation effects and/or changes in atmospheric circulation driven by the buildup of the North American and/or Eurasian ice sheets.

During glacial times, the atmospheric dust load and dust deposition was likely substantially larger, particularly at the southern margins of the Northern Hemisphere ice sheets and over Siberia (Harrison et al., 2001; Lambert et al., 2015; Mahowald et al., 2006). Modelling studies have shown that the buildup of ice over Siberia can be strongly impacted by the effect of dust on the surface albedo, through which an increase of dust deposition on the snow cover leads to a lowering of the snow albedo that in turn leads to higher melt rates (Krinner et al., 2006; Willeit and Ganopolski, 2018).

Continental ice sheets have a strong impact on the climate. It was already recognized by Sanberg and Oerlemans (1983) that under the influence of a preferred wind direction, an ice sheet can create a distinct asymmetry with high precipitation rates at the windward side and low precipitation rates on the leeward-side. This precipitation shadow effect has also been proposed as an explanation for a westward migration of the Eurasian ice sheets during the last glacial period (Liakka et al., 2016, and references therein). Through the precipitation shadow effect, the buildup of the Eurasian Ice Sheet would lead to dry conditions in Siberia and potentially prevent the buildup of an ice sheet in the area.

Another way how ice sheets can impact the climate is through their steering effect on the large-scale atmospheric circulation. Broccoli and Manabe (1987) showed that the buildup of the North American ice sheets leads to substantial changes in the mid-tropospheric flow, including a split of the jet-stream around the northern and southern edges of the ice sheet and a resulting increase of summer temperatures over Alaska. Similar impacts of glacial ice sheets on large-scale atmospheric circulation were found in a number of other modelling studies (e.g. Cook and Held, 1988; Roe and Lindzen, 2001; Justino et al., 2006; Abe-Ouchi et al., 2007; Langen and Vinther, 2009; Liakka and Nilsson, 2010; Ullman et al., 2014; Liakka et al., 2016). Generally these studies indicate a warming over Alaska as a result of the growth of the North American ice sheets, but it differs from one study to the next how far westward this warming extends into Siberia. Warming in Alaska and Siberia is linked to increased poleward heat transport induced by changes in the atmospheric stationary waves and to local feedbacks involving the surface albedo and atmospheric water vapor content (Liakka and Lofverstrom, 2018). An independent compilation of LGM temperature reconstructions based on various land proxy data provides support to these inferences showing that LGM summer temperatures in Northern Siberia were overall not very different from the relatively mild present-day temperatures in the region (Meyer et al., 2017).

The lack of Siberian ice coverage during the LGM has often been attributed to the increased atmospheric dust load and/or a precipitation shadow effect of the Eurasian Ice Sheet to the west. However, based on these mechanisms alone one cannot readily explain the absence of a Siberian ice sheet in some glacial periods, but its presence in others, or reconstructions of Siberian LGM summer temperatures close to present-day values (Meyer et al., 2017), suggesting that these processes are likely only part of the story. Existing and new coupled climate model results can shed light on these intriguing geological observations. Here we show that the inter-model spread of simulated LGM summer temperatures is exceptionally large in Siberia compared to any other region, suggesting a high susceptibility of Siberian summer temperatures to minor changes in boundary conditions or model formulation, and discuss potential underlying mechanisms and causes. We will argue that this high susceptibility of Siberian summer temperatures to boundary conditions (hypersensitivity) is a major factor for the absence or presence of ice sheets in different Quaternary glacials.

2 Methodology

In this study we combine LGM simulations from the second and third phases of the Paleoclimate Modelling Intercomparison Project (PMIP2 and PMIP3) with LGM sensitivity experiments using the Community Earth System Model (CESM).

2.1 PMIP experiments

We use 17 LGM coupled climate model simulations from PMIP2 and PMIP3/CMIP5 (Table 1; Braconnot et al., 2007; Harrison et al., 2015) and their corresponding pre-industrial (PI) control simulations as a reference. LGM boundary conditions follow the PMIP2 and PMIP3 protocols and include reduced greenhouse-gas concentrations, changed astronomical parameters, prescribed continental ice sheets and a lower global sea level. Nearly half (7/17) of these simulations include dynamic vegetation while the

https://doi.org/10.5194/cp-2019-58
Preprint. Discussion started: 13 June 2019

remainder uses prescribed PI vegetation (Table 1). See https://pmip2.lsce.ipsl.frandhttps://pmip3.lsce.ipsl.fr for further details and references. The analysis of PMIP model output is based on climatological means and all output was regridded to a common 1° by 1° horizontal resolution. In order to compare the sea-level pressure results from different models and between PI and LGM we removed the global mean before calculating the anomalies.

2.2 CESM experiments

To study the simulated LGM temperatures in the Siberian region in more detail, we analyzed a number of sensitivity experiments performed with the state-of-the-science coupled climate model CESM (version 1.2; Hurrell et al., 2013). The model includes the Community Atmosphere Model (CAM), Community Land Model (CLM4.0), the Parallel Ocean Program (POP2) and the Community Ice Code (CICE4). In all our CESM experiments, we use a horizontal resolution of 2° in the atmosphere (finite volume core) and land, and a nominal 1° resolution of the ocean (60 levels in the vertical) and sea-ice models with a displaced North Pole.

For the CESM LGM simulations we followed the most recent PMIP protocol (PMIP4; Kageyama et al., 2017), including greenhouse-gas concentrations (190 ppm CO_2, 357 ppb CH_4 and 200 ppb N_2O), orbital parameters (eccentricity of 0.019, obliquity of 22.949° and perihelion-180° of 114.42°) and changes in the land-sea distribution and altitude due to lower sea-level (Di Nezio et al., 2018). In this study we used as default the GLAC-1D LGM ice sheet reconstruction (Tarasov et al., 2012; Briggs et al., 2014). Note that the PMIP4 CH_4 concentration of 375 ppb is slightly higher than the one used here.

The land model CLM4.0 includes the possibility to use a representation of the carbon-nitrogen cycle and to calculate per plant-functional-type the resulting changes in leaf area index, stem area index and vegetation heights (Lawrence et al., 2011). These changes in the biophysical properties of the vegetation cover impact, for instance, evapotranspiration and surface albedo. Note that the spatial distribution of plant-functional-types is prescribed in CLM4.0, which is why the model is sometimes described as a semi-dynamic vegetation model. Nonetheless, in the remainder of this manuscript we will refer to simulations that include carbon-nitrogen dynamics as 'interactive vegetation'. To study the interdependency of interactive vegetation and atmospheric model physics we performed a total of four experiments with either CAM4 or CAM5 and including or excluding interactive vegetation. The simulations testing the impact of interactive vegetation are referred to as the "Interactive vegetation" ensemble (Table 2).

We used two different versions of the atmosphere model, CAM4 and CAM5, to investigate the importance of the atmospheric model physics. CAM5 differs from its predecessor because it simulates indirect aerosol radiative effects by including full aerosol-cloud interactions. Furthermore, it includes improved schemes for moist turbulence, shallow convection and cloud micro- and macro-physics. Finally, while CAM4's grid has 26 vertical levels, in CAM5 four levels were added near the surface for a better representation of boundary layer processes. See Neale et. al. (2010) for a more detailed description of the atmospheric models used in CESM. The simulations testing the impact of atmospheric model physics are referred to as the "Atmospheric model physics" ensemble (Table 2).

In a third ensemble of sensitivity experiments we altered the imposed LGM ice sheet boundary conditions. Within the framework of PMIP4 two LGM ice sheet reconstructions are suggested as boundary conditions for the LGM experiments (Kageyama

https://doi.org/10.5194/cp-2019-58
Preprint. Discussion started: 13 June 2019

et al., 2017), namely GLAC-1D (Tarasov et al., 2012; Briggs et al., 2014) and ICE-6G (Peltier et al., 2015). When comparing these two ice sheet reconstructions we find substantial differences, especially an overall increase of the height of the North American ice sheets in ICE-6G compared to GLAC-1D and a lowering of the Eurasian ice sheet (Figure 5A; both differences are on the order of 10% of the total ice sheet height). To investigate the impact of these two different ice sheet reconstructions on simulated Siberian LGM temperatures, we performed an additional experiment that is identical to the LGM_CAM5_noVeg experiment except that it includes ICE-6G ice sheets (referred to as LGM_CAM5_noVeg_ice6g). The simulations testing the impact of different prescribed continental ice sheets are referred to as the "Continental ice sheets" ensemble (Table 2).

All LGM experiments performed with CESM start from a previous LGM simulation and are run for at least 200 years to obtain a new surface climate equilibrium. Climatologies are calculated based on the last 30 years of the simulations. For the sensitivity experiments studying interactive vegetation and the impact of atmospheric model physics, we also performed corresponding PI simulations (Table 2) to enable a proper analysis of the impacts. Our five CESM LGM experiments are jointly referred to as the CESM LGM ensemble.

Throughout this manuscript we focus on summer (June-July-August; JJA) near-surface air temperatures (referred to simply as 'temperatures' in the remainder of this manuscript) as these determine if perennial snow and thus eventually ice caps develop or not. Moreover, when calculating LGM anomalies, we refer to the difference between an LGM simulation and the corresponding PMIP or CESM PI experiment (Table 2). It is in turn differences between these CESM LGM anomalies that we use to highlight mechanisms behind the susceptibility of Siberian summer temperatures (Section 3.2).

3 Results

3.1 Siberian LGM temperatures in PMIP2 and PMIP3 ensemble

The combined PMIP2 and PMIP3 LGM experiments reveal the particularity of LGM JJA temperatures in Siberia. Of all continental areas that were not covered by large ice sheets, Siberia shows the largest inter-model spread (standard deviation; Figure 1B). This large spread in simulated temperatures in the Siberian region is also found in other seasons (not shown). Another striking feature of the Siberian region is that it is one of the few regions where the PMIP multi-model mean temperature anomaly is close to, or even above zero in some areas (Krinner et al., 2006), indicating that LGM summers were as warm as at present (Figure 1A). Taken together, PMIP simulations show LGM JJA temperatures in Siberia ranging from warmer to substantially colder than at present. If we define a target region for Siberia based on the area where the PMIP multi-model spread is larger than 7°C (green contour in Figure 1B; referred to as "Siberian target region" in the remainder of the manuscript), we see that JJA temperature anomalies of the individual models range between -12°C and +12°C (Figure 2).

Disentangling the causes of the particularity of the Siberian LGM summer temperatures based on PMIP results isn't straightforward because of multiple possible underlying causes; nonetheless, some aspects can be identified. Whereas the simulated temperature changes are quite different among PMIP models, a robust decrease in precipitation on the order of 20-30% is simulated (Figure 1C and 1D). As a consequence, the (Pearson) correlation between temperature change and precipitation change is insignificant at the 0.05 significance level (R=0.36; Figure 2A; note that throughout the manuscript, correlation refers to

https://doi.org/10.5194/cp-2019-58
Preprint. Discussion started: 13 June 2019

inter-model correlation). A significant correlation is found between temperature and snow cover, with higher temperatures corresponding to a lower snow cover (R=-0.60; $p<0.05$; Figure 2E). There are similarities between the spatial patterns of the PMIP multi-model spread in temperature anomalies and cloud cover anomalies (Figure 1B and 1F), however, within the Siberian target region local JJA temperature anomalies and cloud cover anomalies are not correlated at the 0.05 significance level (R=-0.45; Figure 2B), arguing against a leading role of local cloud dynamics to explain the large intermodel spread in Siberian temperatures. As in Yanase and Abe-Ouchi (2007), we find that a weakening of the North Pacific high during JJA is a consistent feature of PMIP LGM simulations (Figure 1G). Moreover, a strong correlation is found in the PMIP LGM simulations between JJA temperature and sea-level pressure anomalies over the Siberian target region (R=-0.72; $p<0.05$; Figure 2C): a higher sea-level pressure anomaly corresponds to more negative temperature anomalies. Concurrently, higher sea-level pressure anomalies correspond to more positive cloud cover anomalies (R=0.50; $p<0.05$; Figure 2D). This finding seems at odds with the results of Liakka et al. (2016) who associate higher pressure with lower cloud cover that in turn leads to an increase in JJA temperatures. This suggests that a mechanism different from the one described by Liakka et al. (2016) operates for the majority of PMIP LGM results. The strong negative correlation between JJA temperature and sea-level pressure anomalies suggests that the sea-level pressure changes could be a consequence of local temperature changes, rather than a local forcing. Indeed, another reason for the negative correlation could be a remote forcing through anomalous heat advection into the Siberian target region.

A remote forcing of the temperature variations in the Siberian target region is suggested by correlations between JJA sea-level pressure changes at individual grid points with JJA temperature changes in the Siberian target region. From figure 3 it appears that there are two regions with a significant ($p<0.01$) correlation between grid point JJA sea-level pressure changes and JJA temperature changes averaged over the Siberian target region. The significant negative correlation in the first region, roughly coinciding with the defined Siberian target region, was already discussed above. However, the significant negative correlation in the second region further to the southwest suggests that the magnitude of the deepening of the low-pressure cell over central Asia (White, 1981) controls the amount of warming in the Siberian target region. This relation can be understood as an increased northward advection of heat towards northeastern Siberia as a result of a stronger cyclonic circulation over the central Asian continent.

A deeper understanding of the large multi-model spread in PMIP LGM JJA temperatures over Siberia and of the mechanisms proposed above is hampered by a multitude of differences between PMIP simulations: different model formulations, different parts of the climate system that are included and different boundary conditions because of the uncertainty in the reconstructed LGM ice sheet. Moreover, only a small subset of climate variables is available for a sufficiently large number of the PMIP models to allow for an in-depth analysis. In the following we will therefore investigate a CESM-based ensemble of LGM simulations that has specifically chosen differences between the individual sensitivity experiments and has all climate variables available.

https://doi.org/10.5194/cp-2019-58
Preprint. Discussion started: 13 June 2019

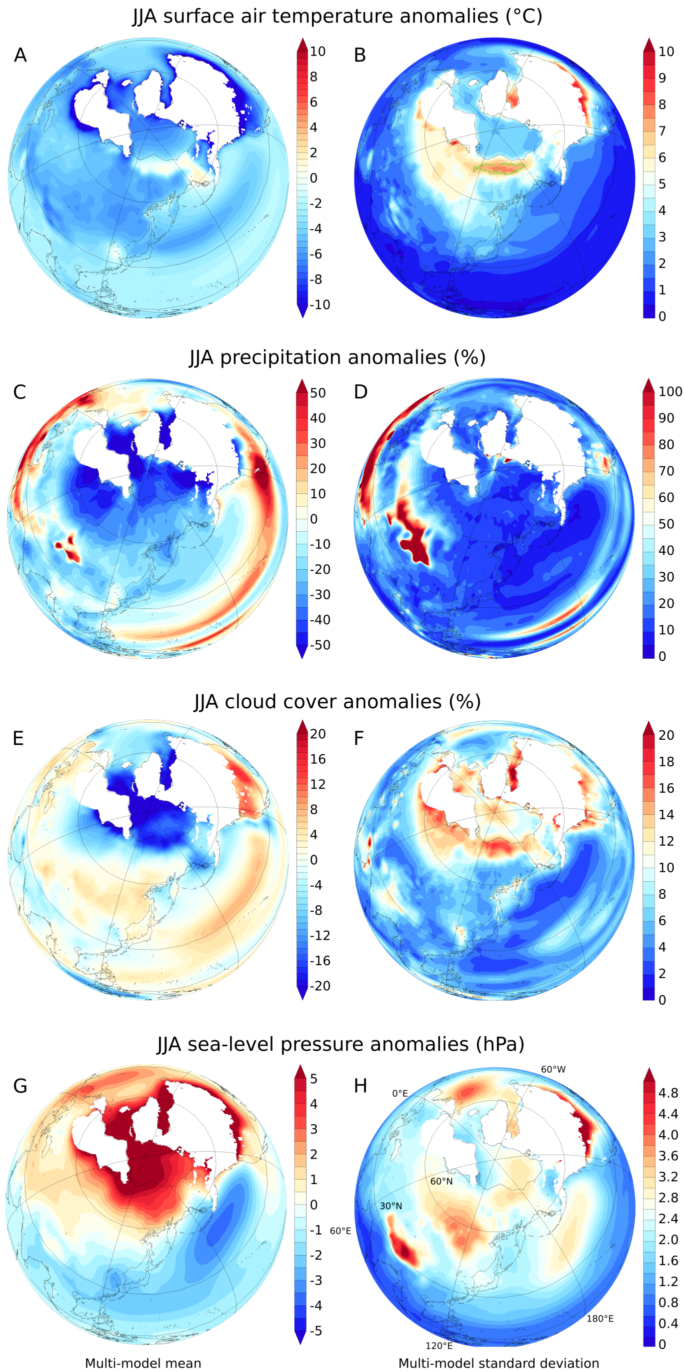

Figure 1. The PMIP2 and PMIP3 multi-model mean (left panels) and multi-model standard deviation (right panels) in LGM JJA climate anomalies. A-B: temperature anomalies (°C). C-D: precipitation anomalies (%). E-F: cloud cover anomalies (%); G-H: sea-level pressure anomalies (hPa). All anomalies are calculated with respect to PI. Note that regions covered by continental ice sheets during the LGM have been masked out. Results are interpolated to a common 1°x1° horizontal grid before calculating the multi-model mean and standard deviation. The green contour in panel B shows the Siberian target region defined here as the region in which the PMIP multi-model standard deviation is larger than 7°C. The black contours denote the LGM coastlines.

https://doi.org/10.5194/cp-2019-58
Preprint. Discussion started: 13 June 2019

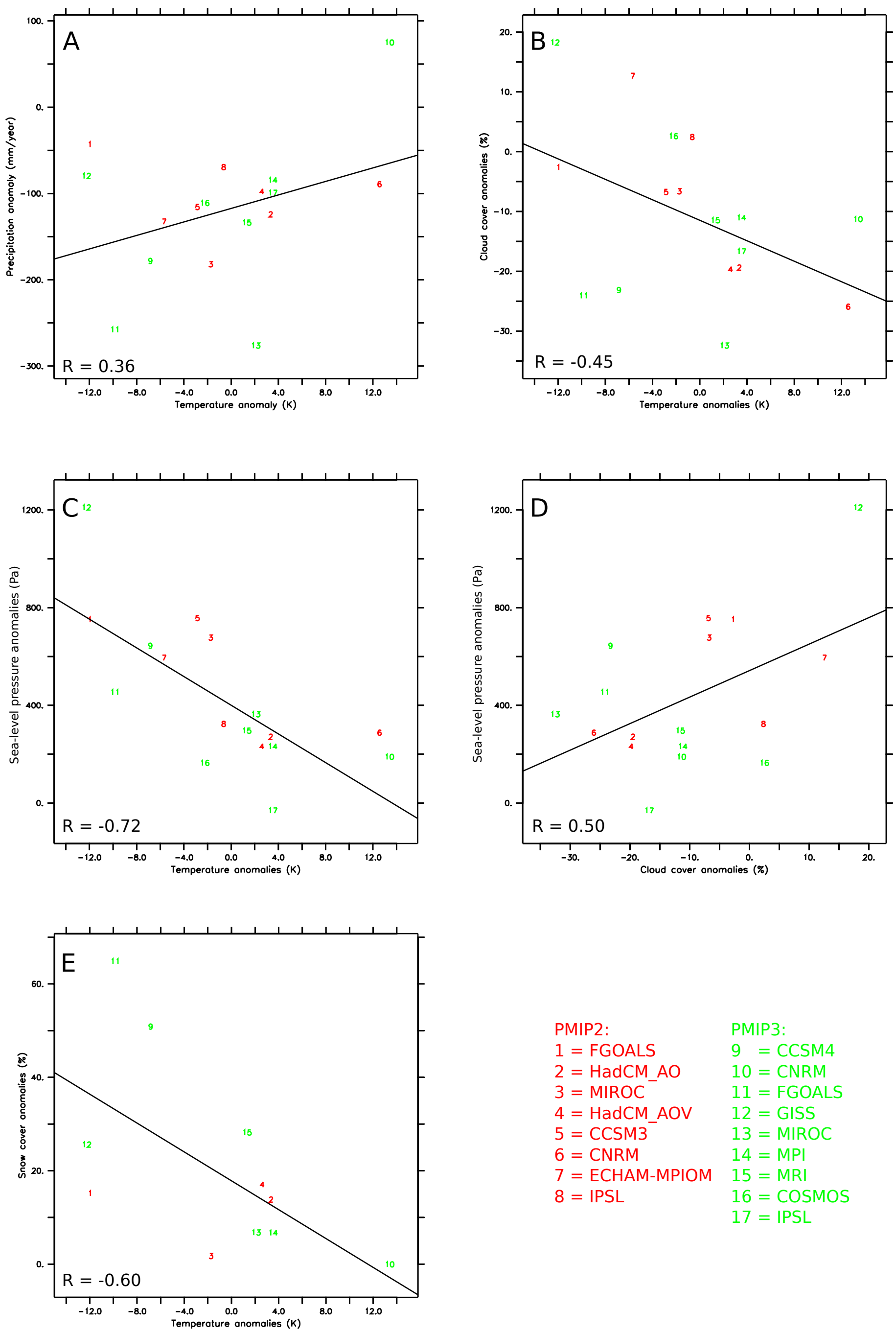

Figure 2. PMIP2 and PMIP3 LGM JJA climate anomalies for the northeast Siberian target region. Red (green) numbers refer to the individual PMIP2 (PMIP3) experiments listed in the lower right. A: Precipitation anomalies ($\mathrm{mm\,year}^{-1}$) versus temperature anomalies (K). B: Cloud cover anomalies (%) versus temperature anomalies (K). C: Sea-level pressure anomalies (Pa) versus temperature anomalies (K). D: Sea-level pressure anomalies (Pa) versus cloud cover anomalies (%). E: Snow cover anomalies (%) versus temperature anomalies (K). Black lines show linear fit and the R-value (Pearson correlation coefficient) is listed in the lower left corner. R-values above 0.49 or below -0.49 indicate a significant correlation ($p<0.05$; t-test).

https://doi.org/10.5194/cp-2019-58
Preprint. Discussion started: 13 June 2019

Climate of the Past Discussions

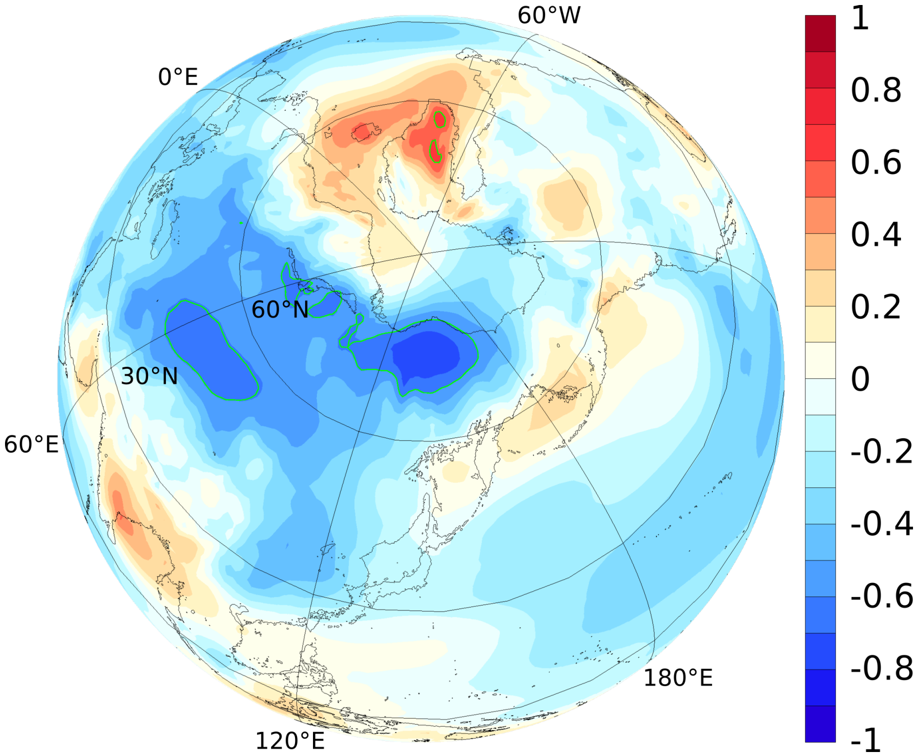

Figure 3. PMIP2 and PMIP3 linear correlations between JJA sea-level pressure anomalies at any given location and JJA temperature anomalies in the Siberian target region (see Figure 1 for the definition). Only for areas bounded by a green contour is the correlation significant (p < 0.01). The black contours denote the LGM coastlines.

https://doi.org/10.5194/cp-2019-58
Preprint. Discussion started: 13 June 2019

3.2 Siberian LGM temperatures in CESM ensemble

We construct three ensembles of LGM sensitivity experiments performed with the CESM climate model in order to investigate in more detail the impact of changes in boundary conditions (continental ice sheets), model formulations (atmospheric model physics) and including different components of the climate system (interactive vegetation; Table 2).

Despite the fact that our CESM LGM ensemble is smaller than the PMIP ensemble (n=5 instead of n=17) and that it wasn't designed to mimic the PMIP ensemble, we find that the spread in the CESM LGM temperature anomalies is surprisingly similar to the PMIP multi-model spread, both in terms of spatial distribution as well as magnitude (Figure 4B). This gives us confidence that investigating the causes of the sensitivity of northeastern Siberian temperatures in the CESM ensemble can provide insights into the PMIP inter-model differences.

First we analyze the "Continental ice sheets" ensemble, consisting of two experiments that only differ in the imposed ice sheet boundary conditions, namely LGM experiments forced by the GLAC-1D (LGM_CAM5_noVeg) or ICE-6G (LGM_CAM5_noVeg_ice6g) ice-sheet reconstructions (Table 2). The LGM simulation using GLAC-1D ice sheets is substantially warmer in northeastern Siberia compared to the simulation using ICE-6G (up to 10°C; Figure 5A). This can only be caused by changes in large-scale atmospheric circulation since the simulations are identical apart from the ice sheets over North America and Eurasia. In line with the PMIP simulations, we find that higher JJA temperatures in the Siberian target region (~3°C) correspond to a decrease of local sea-level pressure (~2 hPa; Figure A1). If we look at changes in the departures from the zonal mean geopotential height at 500hPa (Figure 5), depicting the large-scale Northern Hemisphere stationary wave pattern, we see an increase in geopotential height over Beringia and a decrease over a large area to the west of northeastern Siberia. This results in anomalous 500hPa southerly winds into the area and a corresponding anomalous northward heat transport almost all the way from 30°N to the north pole (Figure 5C). We thus find in CESM a high sensitivity of Siberian JJA temperatures with respect to relatively minor changes in the continental ice sheets which in turn induce changes in the stationary wave pattern and anomalous northward heat transport. The similarity of the associated temperature (Figure 5A) and sea-level pressure anomaly patterns (Figure A1) with the PMIP-based LGM temperature response suggests that this mechanism could clearly explain part of the spread in PMIP simulations.

Another ensemble of CESM LGM simulations, the "Atmospheric model physics" ensemble, is comprised of simulations in which different versions of the atmospheric model were used (CAM4 or CAM5; Table 2). Between the LGM_CAM4_noVeg and LGM_CAM5_noVeg simulations we find changes in large-scale atmospheric circulation, stationary waves and northward heat transport into Siberia (Figure 6) that are very similar to the ones in response to different ice sheets as described above for the "Continental ice sheets" ensemble. However, the resulting surface temperature changes in Siberia are more complex than for the experiments described previously. There is warming in some parts of the region, but substantial parts also show a cooling (Figure 6A). This highlights the complexity of comparing simulations with different atmospheric model versions that not only differ in their response of the large-scale atmospheric circulation to LGM boundary conditions, but also exhibit different local feedbacks with changes in cloud cover, humidity and pressure that are directly influenced by, for instance, differences in cloud parameterizations and radiative properties of the atmosphere.

https://doi.org/10.5194/cp-2019-58
Preprint. Discussion started: 13 June 2019

An important element in the high-latitude climate system is the vegetation-climate feedback. In the PMIP ensemble, 7 out of 17 models include the vegetation-climate feedback (Table 1). However, a systematic difference in simulated JJA LGM temperature anomalies for the Siberian region could not be found when comparing models with vegetation feedback with those that did not include this additional feedback. This doesn't come as a surprise if one considers the relatively small sample size with respect to all the inter-model differences that impact the simulated LGM JJA temperatures. We performed LGM simulations with CESM including and excluding interactive vegetation (the "Interactive vegetation" ensemble; Table 2) to investigate its importance for Siberian temperatures. We find that the vegetation-climate feedback leads to a large LGM JJA cooling over Siberia, which is even more pronounced when using the CAM5 atmospheric model (Figure 7B) instead of CAM4 (Figure 7A). If vegetation is allowed to respond to the changing climate through carbon-nitrogen dynamics, the tree and shrub limits shift south by several degrees of latitude (Figure 8A and 8C). In CESM, the presence of vegetation, its height as well as its density have a large impact on the surface albedo through the vegetation-albedo feedback: vegetation that is higher than the snow pack lowers the surface albedo, increases temperatures, leading to more snow melt, more vegetation growth and an even lower surface albedo. Accordingly, the situation in the CESM simulation including interactive vegetation is such that the cold, dry and snow covered landscape limits vegetation growth and leads to southward migration of the tree and shrub limits. This relationship between vegetation and snow cover also determines the resulting LGM JJA temperature changes (compare figures 7A and 8C). The impact of interactive vegetation is also clearly seen in the PI simulations, resulting in a substantial bias in the leaf area index with respect to the prescribed values (Figure 8A and 8B).

Looking at all the experiments in the "Interactive vegetation" ensemble (Table 2), using different atmospheric model physics (CAM4 versus CAM5; Figure 6) and with or without interactive vegetation (Figure 7), we find that the strong cooling in Siberia in the simulation that combines both the different atmospheric model physics and interactive vegetation (LGM_CAM5_Veg; Figure 7B), is not readily explained as a linear combination of the two individual effects. This shows again the complexity of the response to a combination of factors, in this case changes in large-scale atmospheric circulation, local atmospheric processes and local land-surface processes. It is to be expected that the response of individual PMIP simulations is similarly complex.

https://doi.org/10.5194/cp-2019-58
Preprint. Discussion started: 13 June 2019

Climate of the Past
Discussions
Open Access

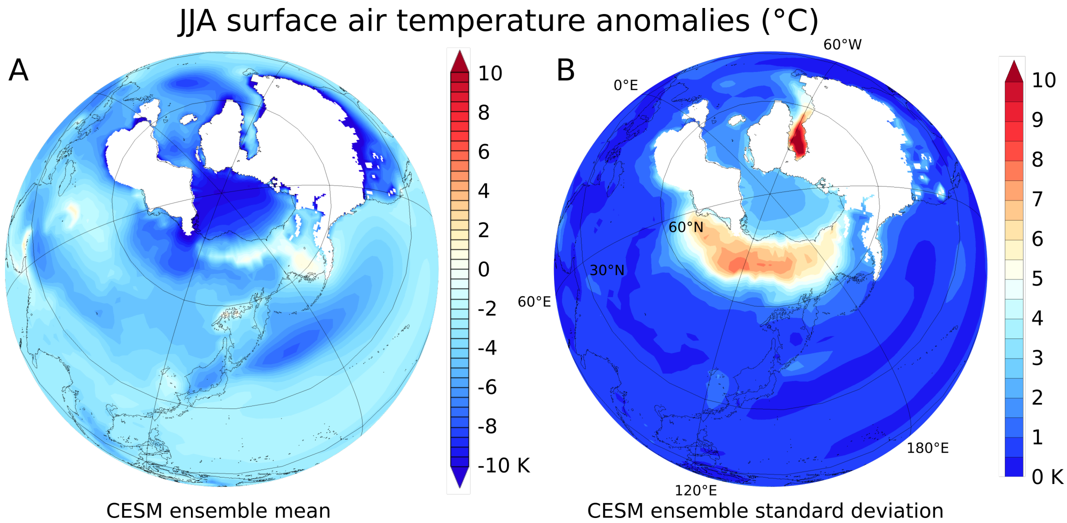

Figure 4. CESM ensemble mean (A) and ensemble standard deviation (B) of LGM JJA temperature anomalies (°C). Note that regions covered by continental ice sheet during the LGM have been masked. The black contours denote the LGM coastlines.

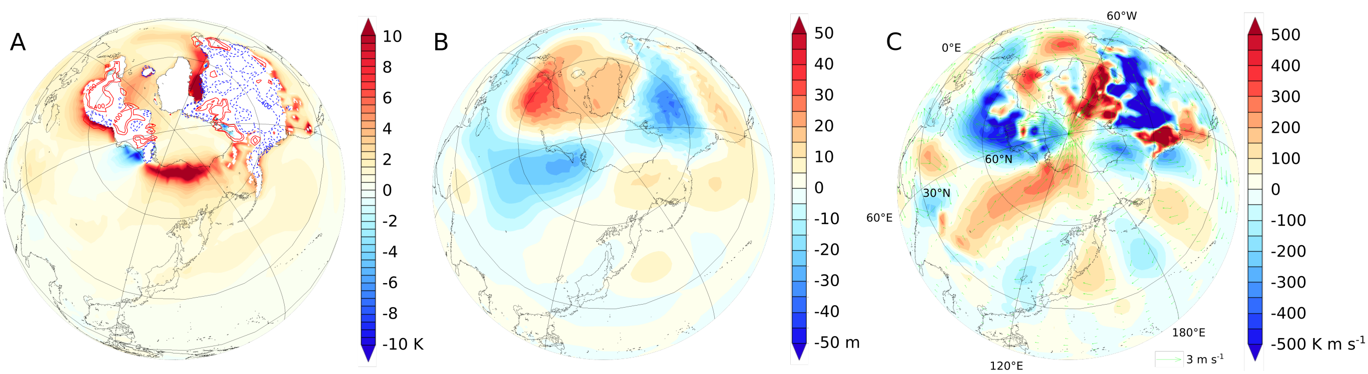

Figure 5. Impact of the prescribed LGM ice-sheet topography (GLAC-1D versus ICE-6G) on simulated LGM climate anomalies during the boreal summer season (JJA). Results are shown as the CESM experiment LGM_CAM5_noVeg minus LGM_CAM5_noVeg_ice6g. A: near-surface temperature anomalies (K). B: 500hPa stationary wave geopotential height anomalies (m; anomalies calculated after subtracting the zonal mean). C: vertically averaged meridional sensible heat transport anomalies ($\mathrm{Kms^{-1}}$; shading). Vectors in panel C show 500 hPa wind anomalies ($\mathrm{ms^{-1}}$). In panel A regions covered by continental ice sheets during the LGM have been masked out. The red (blue) contours in panel A depict positive (negative) differences in ice sheet height (m) between the GLAC-1D and ICE-6G reconstructions (GLAC-1D - ICE-6G; 300 m contour interval). The black contours denote the LGM coastlines.

https://doi.org/10.5194/cp-2019-58
Preprint. Discussion started: 13 June 2019

Climate of the Past Discussions

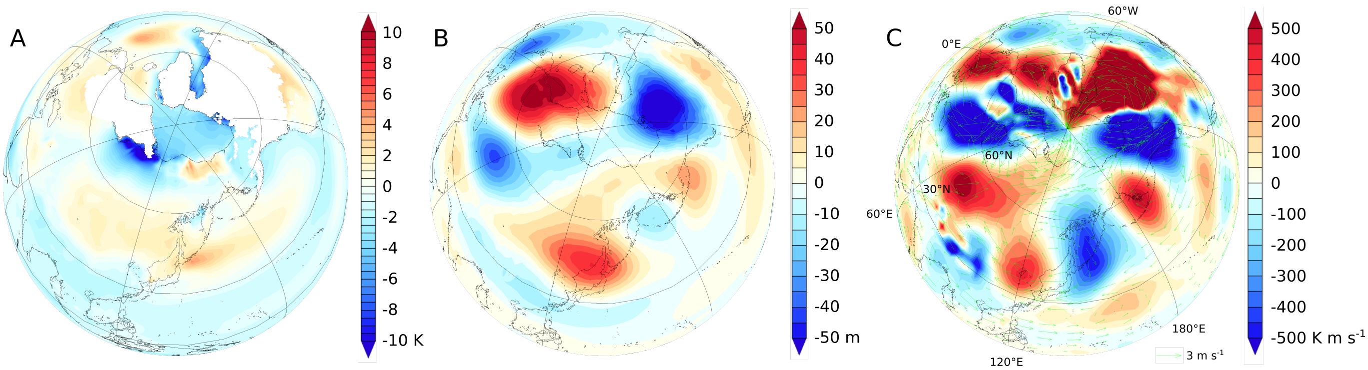

Figure 6. Impact of using a different atmospheric model (CAM5 versus CAM4) on simulated LGM climate anomalies during the boreal summer season (JJA). Results are shown as LGM-PI anomalies for LGM_CAM5_noVeg minus LGM_CAM4_noVeg. A: near-surface temperature anomalies (K). B: 500 hPa stationary wave geopotential height anomalies (m; anomalies calculated after subtracting the zonal mean). C: vertically averaged meridional sensible heat transport anomalies (Kms^{-1}; shading). Vectors in panel C show 500 hPa wind anomalies (ms^{-1}). In panel A regions covered by continental ice sheets during the LGM have been masked out. The black contours denote the LGM coastlines.

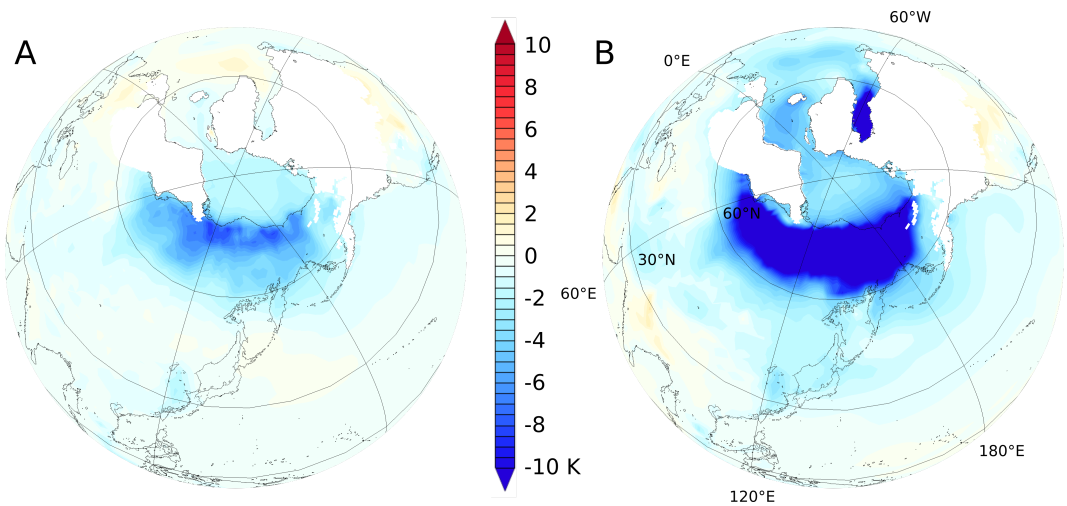

Figure 7. JJA LGM temperature anomalies showing the impact of introducing vegetation-climate feedbacks. Results are shown as LGM-PI anomalies for CAM4 (A; LGM_CAM4_Veg – LGM_CAM4_noVeg) and CAM5 (B; LGM_CAM5_Veg – LGM_CAM5_noVeg). Regions covered by continental ice sheets during the LGM have been masked out. The black contours denote the LGM coastlines.

https://doi.org/10.5194/cp-2019-58
Preprint. Discussion started: 13 June 2019

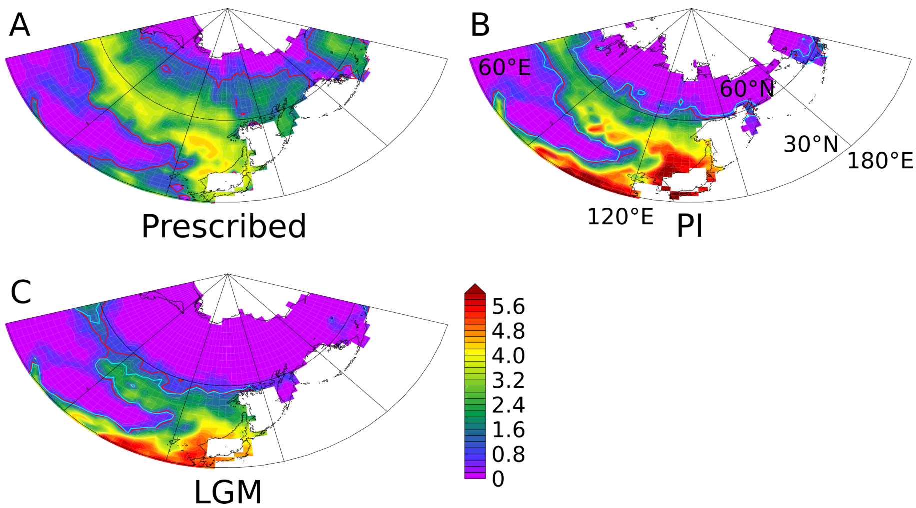

Figure 8. Leaf area index (m^2m^{-2}) in northeastern Asia as prescribed in the simulations without interactive vegetation (A), and as simulated in the pre-industrial (B) and LGM (C) CAM4_Veg experiments including interactive vegetation. Contours give the leaf area index of 1 m^2m^{-2} (red for CAM4 and light blue for CAM5). The black contours denote the LGM coastlines.

4 Concluding remarks

From a climate model perspective, LGM JJA temperatures in Siberia appear highly susceptible to changes in the imposed boundary conditions, included feedbacks and processes, and to the model physics of the different climate model components; much more so for Siberia than for any other region. This becomes apparent from the comparison of 17 different PMIP2 and PMIP3 LGM experiments, as well as from three ensembles of CESM sensitivity experiments. The spread in Siberian JJA LGM temperature anomalies in the CESM ensemble is ~20°C, which is comparable to the inter-model spread of ~24°C found in the PMIP simulations. The main cause appears to be that relatively small changes in the continental ice sheets or model physics can lead to large changes in meridional atmospheric heat transport related to changes in large-scale atmospheric stationary wave patterns, in line with Ullman et al. (2014) and Liakka and Lofverstrom (2018). Local snow-albedo and vegetation-climate feedbacks strongly amplify the initiated Siberian JJA temperature change.

In the examined LGM simulations Siberia receives less precipitation, however, we don't find indications that the buildup of a Siberian ice sheet was hampered by the absence of precipitation. On the contrary, we find that local precipitation and JJA temperature changes are not significantly correlated, while cooler summers are strongly correlated to a higher snow cover, suggesting that a cold climate would be associated with a perennial snow cover. We also do not find support for the notion that changes in large-scale atmospheric stationary wave patterns drive Siberian JJA temperatures directly through local cloud changes.

Although situated at high northern latitudes, geological evidence suggests that Siberia was covered by continental ice sheets during some glacial periods, but remained largely ice free during, for instance, the LGM. Increased atmospheric dust deposition and a precipitation-shadow cast by the Eurasian ice sheets to the west are often highlighted as possible causes, however, such mechanisms cannot readily explain the absence of a Siberian ice sheet in some glacial periods, but its presence in others, nor explain reconstructions of Siberian LGM summer temperatures close to present-day values (Meyer et al., 2017). This is suggesting that these processes are likely only part of the story, and here we argue for the importance of changes in meridional atmospheric heat transport and the exact configuration of northern hemisphere continental ice sheets. The combination of these factors, accompanied by local feedbacks can lead to strongly divergent summer temperatures in the region, which during some glacial periods could be sufficiently low to allow for the buildup of an ice sheet, while during other glacials, above-freezing summer temperatures will prevent a multi-year snow-pack, and hence an ice sheet, from forming.

Data availability. For the PMIP experiment results see https://pmip2.lsce.ipsl.frandhttps://pmip3.lsce.ipsl.fr for further details and references. Results from the CESM sensitivity experiments can be obtained from the authors.

Author contributions. P. B. and I. R. designed the study. P. B. performed the CESM sensitivity experiments and analysed the PMIP and CESM experiments. P. B. wrote the manuscript. I. R. reviewed the literature for geological and climatological reconstructions. All authors participated in the discussion of the results and the manuscript, and provided feedback and comments.

Competing interests. The authors declare that they have no conflict of interest.

Acknowledgements. This study is a contribution to the PalMod project funded by the German Federal Ministry of Education and Science (BMBF). The climate model simulations were carried out on the supercomputer of the Norddeutscher Verbund für Hoch- und Höchstleistungsrechnen (HLRN). We thank Pedro diNezio for providing us with CESM LGM initial and boundary conditions.

References

Abe-Ouchi, A., Segawa, T., and Saito, F.: Climatic conditions for modelling the Northern Hemisphere ice sheets throughout the ice age cycle, Climate of the Past, 3, 423–438, https://doi.org/10.5194/cp-3-423-2007, 2007.

Abe-Ouchi, A., Saito, F., Kawamura, K., Raymo, M. E., Okuno, J., Takahashi, K., and Blatter, H.: Insolation-driven 100,000-year glacial cycles and hysteresis of ice-sheet volume, Nature, 500, 190–193, https://doi.org/10.1038/nature12374, http://dx.doi.org/10.1038/nature12374, 2013.

Adler, R. E., Polyak, L., Ortiz, J. D., Kaufman, D. S., Channell, J. E. T., Xuan, C., Grottoli, A. G., Sellén, E., and Crawford, K. A.: Sediment record from the western Arctic Ocean with an improved Late Quaternary age resolution : HOTRAX core HLY0503-8JPC , Mendeleev Ridge, Global and Planetary Change, 68, 18–29, https://doi.org/10.1016/j.gloplacha.2009.03.026, http://dx.doi.org/10.1016/j.gloplacha.2009.03.026, 2009.

Backman, J., Fornaciari, E., and Rio, D.: Marine Micropaleontology Biochronology and paleoceanography of late Pleistocene and Holocene calcareous nannofossil abundances across the Arctic Basin, Marine Micropaleontology, 72, 86–98, https://doi.org/10.1016/j.marmicro.2009.04.001, http://dx.doi.org/10.1016/j.marmicro.2009.04.001, 2009.

Basilyan, A. E., Nikolsky, P. A., Maksimov, F. E., and Kuznetsov, V. Y.: Age of Cover Glaciation of the New Siberian Islands Based on 230Th/U-dating of Mollusk Shells, Structure and Development of the Lithosphere, Paulsen, pp. 506–514, 2010.

Beghin, P., Charbit, S., Dumas, C., Kageyama, M., Roche, D. M., and Ritz, C.: Interdependence of the growth of the Northern Hemisphere ice sheets during the last glaciation: the role of atmospheric circulation, Climate of the Past, 10, 345–358, https://doi.org/10.5194/cp-10-345-2014, 2014.

Boucsein, B., Knies, J., and Stein, R.: Organic matter deposition along the Kara and Laptev Seas continental margin (eastern Arctic Ocean) during last deglaciation and Holocene : evidence from organic geochemical and petrographical data, Marine Geology, 183, 67–87, 2002.

Braconnot, P., Otto-Bliesner, B. L., Harrison, S. P., Joussaume, S., Peterchmitt, J.-Y., Abe-Ouchi, A., Crucifix, M., Driesschaert, E., Fichefet, T., Hewitt, C. D., Kageyama, M., Kitoh, A., Laîné, A., Loutre, M.-F., Marti, O., Merkel, U., Ramstein, G., Valdes, P., Weber, S. L., Yu, Y., and Zhao, Y.: Results of PMIP2 coupled simulations of the Mid-Holocene and Last Glacial Maximum - Part 1: experiments and large-scale features, Climate of the Past, 3, 261–277, 2007.

Briggs, R. D., Pollard, D., and Tarasov, L.: A data-constrained large ensemble analysis of Antarctic evolution since the Eemian, Quaternary Science Reviews, 103, 91–115, https://doi.org/10.1016/j.quascirev.2014.09.003, http://dx.doi.org/10.1016/j.quascirev.2014.09.003, 2014.

Broccoli, A. J. and Manabe, S.: The Effects of the Laurentide Ice Sheet on North American Climate during the Last Glacial Maximum, Géographie physique et Quaternaire, 41, 291–299, https://doi.org/10.7202/032684ar, http://www.erudit.org/revue/gpq/1987/v41/n2/032684ar.html, 1987.

Charbit, S., Ritz, C., Philippon, G., Peyaud, V., and Kageyama, M.: Numerical reconstructions of the Northern Hemisphere ice sheets through the last glacial-interglacial cycle, Climate of the Past, 3, https://doi.org/10.5194/cpd-2-879-2006, 2007.

Cook, K. H. and Held, I. M.: Stationary Waves of the Ice Age Climate, https://doi.org/10.1175/1520-0442(1988)001<0807:swotia>2.0.co;2, 1988.

Darby, D. A., Polyak, L., and Bauch, H. A.: Progress in Oceanography Past glacial and interglacial conditions in the Arctic Ocean and marginal seas – a review, 71, 129–144, https://doi.org/10.1016/j.pocean.2006.09.009, 2006.

Di Nezio, P. N., Tierney, J. E., Otto-Bliesner, B. L., Timmermann, A., Bhattacharya, T., Rosenbloom, N., and Brady, E.: Glacial changes in tropical climate amplified by the Indian Ocean, Science Advances, 4, 1–12, https://doi.org/10.1126/sciadv.aat9658, 2018.

Ehlers, J., Gibbard, P. L., and Hughes, P. D.: Quaternary Glaciations and Chronology, in: Past Glacial Environments, edited by Menzies, J. and van der Meer, J. J. M., chap. 4, Elsevier, 2018.

Ganopolski, A., Calov, R., and Claussen, M.: Simulation of the last glacial cycle with a coupled climate ice-sheet model of intermediate complexity, Climate of the Past, 6, 229–244, https://doi.org/10.5194/cp-6-229-2010, 2010.

Gualtieri, L., Vartanyan, S. L., Brigham-Grette, J., and Anderson, P. M.: Evidence for an ice-free Wrangel Island, northeast Siberia during the Last Glacial Maximum, Boreas, 34, 264–273, https://doi.org/10.1080/03009480510013097, 2005.

Harrison, S. P., Kohfeld, K. E., Roelandt, C., and Claquin, T.: The role of dust in climate changes today, at the last glacial maximum and in the future, Earth-Science Reviews, 54, 43–80, https://doi.org/10.1016/S0012-8252(01)00041-1, 2001.

Harrison, S. P., Bartlein, P. J., Izumi, K., Li, G., Annan, J. D., Hargreaves, J. C., Braconnot, P., and Kageyama, M.: Evaluation of CMIP5 palaeo-simulations to improve climate projections, Nature Climate Change, 5, 735–743, https://doi.org/10.1038/nclimate2649, http://www.nature.com/doifinder/10.1038/nclimate2649, 2015.

Hubberten, H. W., Andreev, A., Astakhov, V. I., Demidov, I., Dowdeswell, J. A., Henriksen, M., Hjort, C., Houmark-nielsen, M., Jakobsson, M., Kuzmina, S., Larsen, E., Pekka, J., Lys, A., Saarnisto, M., Schirrmeister, L., Sher, A. V., Siegert, C., Siegert, M. J., and Inge, J.: The periglacial climate and environment in northern Eurasia during the Last Glaciation, 23, 1333–1357, https://doi.org/10.1016/j.quascirev.2003.12.012, 2004.

Hurrell, J. W., Holland, M. M., Gent, P. R., Ghan, S., Kay, J. E., Kushner, P. J., Lamarque, J. F., Large, W. G., Lawrence, D. M., Lindsay, K., Lipscomb, W. H., Long, M. C., Mahowald, N. M., Marsh, D. R., Neale, R. B., Rasch, P., Vavrus, S., Vertenstein, M., Bader, D. A., Collins, W. D., Hack, J. J., Kiehl, J., and Marshall, S.: The community earth system model: A framework for collaborative research, Bulletin of the American Meteorological Society, 94, 1339–1360, https://doi.org/10.1175/BAMS-D-12-00121.1, 2013.

Jakobsson, M., Andreassen, K., Rún, L., Dove, D., Dowdeswell, J. A., England, J. H., Funder, S., Hogan, K., Ingólfsson, Ó., Jennings, A., Krog, N., Kirchner, N., Landvik, J. Y., Mayer, L., Mikkelsen, N., Möller, P., Niessen, F., Nilsson, J., Regan, M. O., Polyak, L., and Nørgaard-pedersen, N.: Arctic Ocean glacial history, Quaternary Science Reviews, 92, 40–67, https://doi.org/10.1016/j.quascirev.2013.07.033, http://dx.doi.org/10.1016/j.quascirev.2013.07.033, 2014.

Jakobsson, M., Nilsson, J., Anderson, L. G., Backman, J., Björk, G., Cronin, T. M., Kirchner, N., Koshurnikov, A., Mayer, L., Noormets, R., O'Regan, M., Stranne, C., Ananiev, R., Barrientos Macho, N., Cherniykh, D., Coxall, H., Eriksson, B., Flodén, T., Gemery, L., Gustafsson, Ö., Jerram, K., Johansson, C., Khortov, A., Mohammad, R., and Semiletov, I.: Evidence for an ice shelf covering the central Arctic Ocean during the penultimate glaciation, Nature Communications, 7, 1–10, https://doi.org/10.1038/ncomms10365, 2016.

Justino, F., Timmermann, A., Merkel, U., and Peltier, W. R.: An initial intercomparison of atmospheric and oceanic climatology for the ICE-5G and ICE-4G models of LGM paleotopography, Journal of Climate, 19, 3–14, https://doi.org/10.1175/JCLI3603.1, 2006.

Kageyama, M., Albani, S., Braconnot, P., Harrison, S. P., Hopcroft, P. O., Ivanovic, R. F., Lambert, F., Marti, O., Peltier, W. R., Peterschmitt, J. Y., Roche, D. M., Tarasov, L., Zhang, X., Brady, E. C., Haywood, A. M., LeGrande, A. N., Lunt, D. J., Mahowald, N. M., Mikolajewicz, U., Nisancioglu, K. H., Otto-Bliesner, B. L., Renssen, H., Tomas, R. A., Zhang, Q., Abe-Ouchi, A., Bartlein, P. J., Cao, J., Li, Q., Lohmann, G., Ohgaito, R., Shi, X., Volodin, E., Yoshida, K., Zhang, X., and Zheng, W.: The PMIP4 contribution to CMIP6 – Part 4: Scientific objectives and experimental design of the PMIP4-CMIP6 Last Glacial Maximum experiments and PMIP4 sensitivity experiments, Geoscientific Model Development, 10, 4035–4055, https://doi.org/10.5194/gmd-10-4035-2017, 2017.

Kleman, J., Fastook, J., Ebert, K., Nilsson, J., and Caballero, R.: Pre-LGM northern hemisphere ice sheet topography, Climate of the Past, 9, 2365–2378, https://doi.org/10.5194/cp-9-2365-2013, 2013.

Krinner, G., Boucher, O., and Balkanski, Y.: Ice-free glacial northern Asia due to dust deposition on snow, Climate Dynamics, 27, 613–625, https://doi.org/10.1007/s00382-006-0159-z, 2006.

Lambert, F., Tagliabue, A., Shaffer, G., Lamy, F., Winckler, G., Farias, L., Gallardo, L., and Pol-holz, R. D.: Dust fluxes and iron fertilization in Holocene and Last Glacial Maximum climates, Geophyscial Research Letters, pp. 6014–6023, https://doi.org/10.1002/2015GL064250.Received, 2015.

Langen, P. L. and Vinther, B. M.: Response in atmospheric circulation and sources of Greenland precipitation to glacial boundary conditions, Climate Dynamics, 32, 1035–1054, https://doi.org/10.1007/s00382-008-0438-y, 2009.

Lawrence, D. M., Oleson, K. W., Flanner, M. G., Thornton, P. E., Swenson, S. C., Lawrence, P. J., Zeng, X., Yang, Z.-L., Levis, S., Sakaguchi, K., Bonan, G. B., and Slater, A. G.: Parameterization improvements and functional and structural advances in Version 4 of the Community Land Model, Journal of Advances in Modeling Earth Systems, 3, 1–27, https://doi.org/10.1029/2011ms000045, 2011.

Liakka, J. and Lofverstrom, M.: Arctic warming induced by the Laurentide ice sheet topography, Climate of the Past, 14, 887–900, https://doi.org/10.5194/cp-2018-26, https://www.clim-past-discuss.net/cp-2018-26/, 2018.

Liakka, J. and Nilsson, J.: The impact of topographically forced stationary waves on local ice-sheet climate, Journal of Glaciology, 56, 534–544, https://doi.org/10.3189/002214310792447824, 2010.

Liakka, J., Colleoni, F., and Lofverstrom, M.: The impact of the North American glacial topography on the evolution of the Eurasian ice sheet during the last glacial cycle, Climate of the Past, 12, 1225–1241, https://doi.org/10.5194/cp-12-1225-2016, 2016.

Mahowald, N. M., Yoshioka, M., Collins, W. D., Conley, A. J., Fillmore, D. W., and Coleman, D. B.: Climate response and radiative forcing from mineral aerosols during the last glacial maximum, pre-industrial, current and doubled-carbon dioxide climates, Geophysical Research Letters, 33, 2–5, https://doi.org/10.1029/2006GL026126, 2006.

Meyer, V. D., Hefter, J., Lohmann, G., Max, L., Tiedemann, R., and Mollenhauer, G.: Summer temperature evolution on the Kamchatka Peninsula, Russian Far East, during the past 20â€000 years, Climate of the Past, 13, 359–377, https://doi.org/10.5194/cp-13-359-2017, 2017.

Niessen, F., Hong, J. K., Hegewald, A., Matthiessen, J., Stein, R., Kim, H., Kim, S., Jensen, L., Jokat, W., Nam, S. I., and Kang, S. H.: Repeated Pleistocene glaciation of the East Siberian continental margin, Nature Geoscience, 6, 842–846, https://doi.org/10.1038/ngeo1904, http://dx.doi.org/10.1038/ngeo1904, 2013.

Patton, H., Andreassen, K., Bjarnadóttir, L. R., Dowdeswell, J. A., Winsborrow, M. C. M., Noormets, R., Polyak, L., Auriac, A., and Hubbard, A.: Geophysical constraints on the dynamics and retreat of the Barents Sea ice sheet as a paleobenchmark for models of marine ice sheet deglaciation, Reviews of Geophysics, 53, 1051–1098, https://doi.org/10.1002/2015RG000495.Received, 2015.

Peltier, W. R., Argus, D. F., and Drummond, R.: Journal of Geophysical Research : Solid Earth, Journal of Geophysical Research: Solid Earth, 2015, 450–487, https://doi.org/10.1002/2014JB011176.Received, 2015.

Pitulko, V. V., Nikolsky, P. A., Girya, E. Y., and Basilyan, A. E.: The Yana RHS Site : Humans in the Arctic before the last glacial maximum, Science, 303, https://doi.org/10.1126/science.1085219, 2004.

Polyak, L., Curry, W. B., Darby, D. A., Bischof, J., and Cronin, T. M.: Contrasting glacial / interglacial regimes in the western Arctic Ocean as exempli ¢ ed by a sedimentary record from the Mendeleev Ridge, 203, https://doi.org/10.1016/S0031-0182(03)00661-8, 2004.

Polyak, L., Darby, D. A., Bischof, J. F., and Jakobsson, M.: Stratigraphic constraints on late Pleistocene glacial erosion and deglaciation of the Chukchi margin , Arctic Ocean, 67, 234–245, https://doi.org/10.1016/j.yqres.2006.08.001, 2007.

https://doi.org/10.5194/cp-2019-58
Preprint. Discussion started: 13 June 2019

Polyak, L., Bischof, J., Ortiz, J. D., Darby, D. A., Channell, J. E. T., Xuan, C., Kaufman, D. S., Løvlie, R., Schneider, D. A., Eberl, D. D., Adler, R. E., and Council, E. A.: Late Quaternary stratigraphy and sedimentation patterns in the western Arctic Ocean, 68, 5–17, https://doi.org/10.1016/j.gloplacha.2009.03.014, http://dx.doi.org/10.1016/j.gloplacha.2009.03.014, 2009.

Roe, G. H. and Lindzen, R. S.: A one-dimensional model for the interaction between continental-scale ice sheets and atmospheric stationary waves, Climate Dynamics, 17, 479–487, https://doi.org/10.1007/s003820000123, http://link.springer.com/10.1007/s003820000123, 2001.

Sanberg, J. A. M. and Oerlemans, J.: Modelling of Pleistocene European ice sheets: the effect of upslope precipitation, Geologie en Mijnbouw, 1983.

Schirrmeister, L.: Th / U Dating of Frozen Peat , Bol ' shoy Lyakhovsky Island (Northern Siberia), 258, 253–258, https://doi.org/10.1006/qres.2001.2306, 2002.

Stauch, G. and Gualtieri, L.: Late Quaternary glaciations in northeastern Russia, 23, 545–558, https://doi.org/10.1002/jqs, 2008.

Svendsen, J. I., Alexanderson, H., Astakhov, V. I., Demidov, I., Dowdeswell, J. A., Funder, S., Gataullin, V., Henriksen, M., Hjort, C., Houmark-Nielsen, M., Hubberten, H. W., Ingólfsson, l., Jakobsson, M., Kjaer, K. H., Larsen, E., Lokrantz, H., Lunkka, J. P., Lyså, A., Mangerud, J., Matiouchkov, A., Murray, A., Möller, P., Niessen, F., Nikolskaya, O., Polyak, L., Saarnisto, M., Siegert, C., Siegert, M. J., Spielhagen, R. F., and Stein, R.: Late Quaternary ice sheet history of northern Eurasia, Quaternary Science Reviews, 23, 1229–1271, https://doi.org/10.1016/j.quascirev.2003.12.008, 2004.

Tarasov, L., Dyke, A. S., Neal, R. M., and Peltier, W. R.: A data-calibrated distribution of deglacial chronologies for the North American ice complex from glaciological modeling, Earth and Planetary Science Letters, 315-316, 30–40, https://doi.org/10.1016/j.epsl.2011.09.010, http://dx.doi.org/10.1016/j.epsl.2011.09.010, 2012.

Ullman, D. J., Legrande, A. N., Carlson, A. E., Anslow, F. S., and Licciardi, J. M.: Assessing the impact of laurentide ice sheet topography on glacial climate, Climate of the Past, 10, 487–507, https://doi.org/10.5194/cp-10-487-2014, 2014.

Wetterich, S., Rudaya, N., Tumskoy, V., Andreev, A. A., Opel, T., Schirrmeister, L., and Meyer, H.: Last Glacial Maximum records in permafrost of the East Siberian Arctic, Quaternary Science Reviews, 30, 3139–3151, https://doi.org/10.1016/j.quascirev.2011.07.020, http://dx.doi.org/10.1016/j.quascirev.2011.07.020, 2011.

White, G. H.: An observational study of the Northern Hemisphere extratropical summertime general circulation, Journal of the Atmospheric Sciences, 39, 1981.

Willeit, M. and Ganopolski, A.: The importance of snow albedo for ice sheet evolution over the last glacial cycle, Climate of the Past, 14, 697–707, https://doi.org/10.5194/cp-14-697-2018, 2018.

Yanase, W. and Abe-Ouchi, A.: The LGM surface climate and atmospheric circulation over East Asia and the North Pacific in the PMIP2 coupled model simulations, Climate of the Past, 3, 439–451, https://doi.org/10.5194/cp-3-439-2007, 2007.

https://doi.org/10.5194/cp-2019-58
Preprint. Discussion started: 13 June 2019

Climate of the Past
Discussions

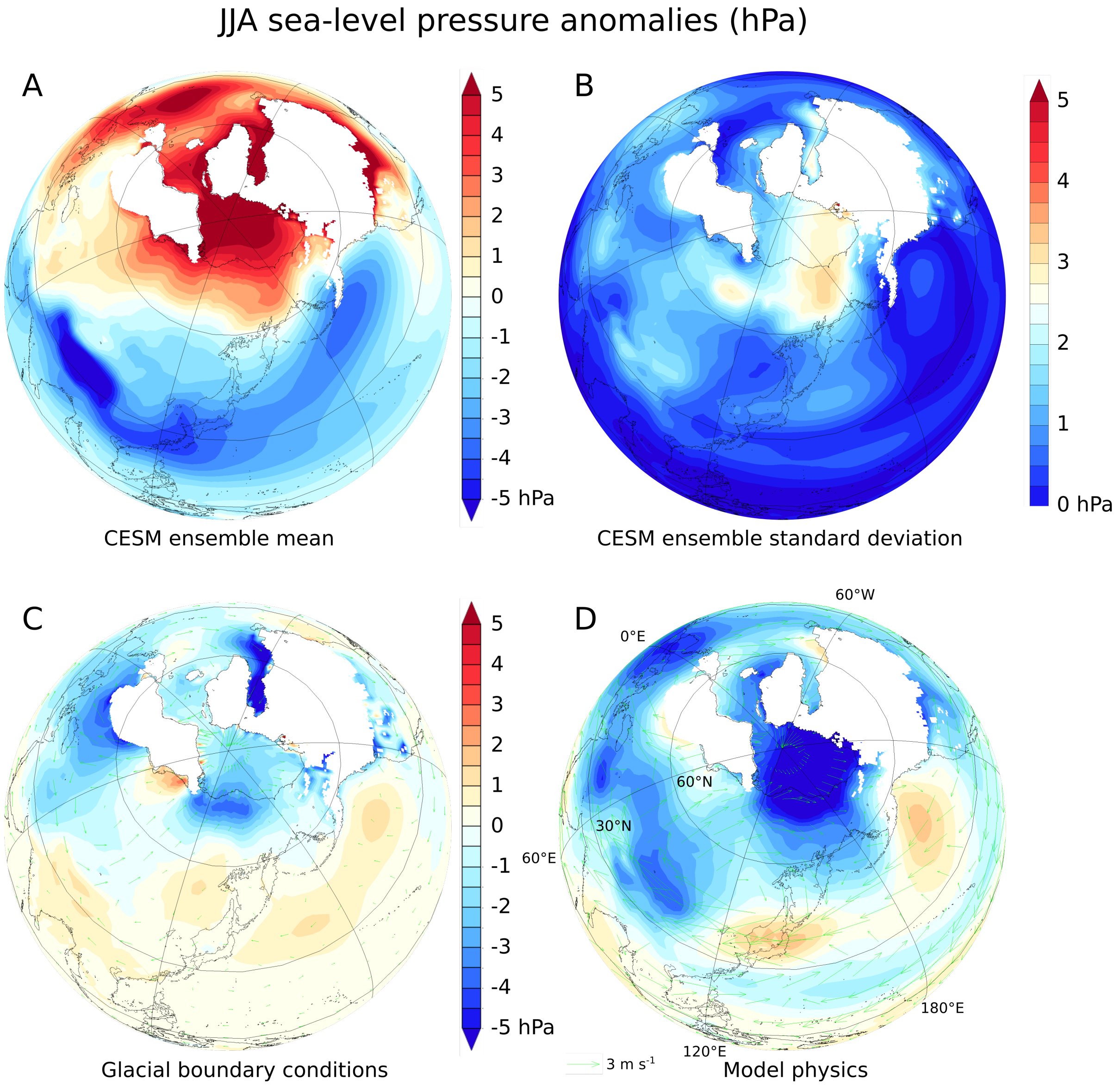

Figure A1. JJA LGM sea level pressure (SLP) anomalies (hPa). The CESM ensemble mean (A) and standard deviation (B) over all CESM experiments, and anomalies showing the impact of the prescribed LGM ice-sheet topography (C; GLAC-1D minus ICE-6G) or of using a different atmospheric model (D; CAM5 minus CAM4). Vectors in panels C and D show 500 hPa wind anomalies (ms^{-1}). Regions covered by continental ice sheets during the LGM have been masked out. The black contours give the LGM coastlines.

https://doi.org/10.5194/cp-2019-58
Preprint. Discussion started: 13 June 2019

Table 1. List with PMIP2 and PMIP3 climate models included in the analysis with details on grid resolution and usage of interactive vegetation. The following abbreviations are used: Atm (atmospheric grid resolution), Ocn (ocean grid resolution), L (number of levels in the vertical). See https://pmip2.lsce.ipsl.fr and https://pmip3.lsce.ipsl.fr for further details and references.

Model	Institution	Grid Resolution	Interactive vegetation	PMIP phase
CCSM3	National Center for Atmospheric Research, USA	Atm: 128 x 64 x L26 Ocn: 320 x 384 x L40	No	2
CNRM-CM3.3	Centre National de Recherches Meteorologiques, France	Atm: 256 x 128 x L31 Ocn: 362 x 292 x L42	No	2
ECHAM5-MPIOM	Max Planck Institute for Meteorology, Germany	Atm: 96 x 48 x L19 Ocn: 120 x 101 x L40	Yes	2
FGOALS1.0_g	LASG/Institute of Atmospheric Physics, China	Atm: 128 x 60 x L26 Ocn: 360 x 180 x L33	No	2
HadCM3_AO	UK Met Office Hadley Centre, UK	Atm: 96 x 72 x L19 Ocn: 288 x 144 x L20	No	2
HadCM3_AOV	UK Met Office Hadley Centre, UK	Atm: 96 x 72 x L19 Ocn: 288 x 144 x L20	Yes	2
IPSL-CM4_v1	Institut Pierre Simon Laplace, France	Atm: 96 x 72 x L19 Ocn: 182 x 149 x L31	No	2
MIROC3.2.2	Center for Climate System Research, JAMSTEC, Japan	Atm: 128 x 64 x L20 Ocn: 256 x 192 x L43	No	2
CCSM4	National Center for Atmospheric Research, USA	Atm: 288 x 192 x L26 Ocn: 320 x 384 x L60	Yes	3
CNRM-CM5	CNRM - C. Européen de Rech. Formation Avancée Calcul Sci.	Atm: 256 x 128 x L31 Ocn: 362 x 292 x L42	No	3
COSMOS-ASO	Max Planck Institute for Meteorology, Germany	Atm: 96 x 48 x L19 Ocn: 120 x 101 x L40	Yes	3
FGOALS_g2	ASG/Institute of Atmospheric Physics, China	Atm: 128 x 60 x L26 Ocn: 360 x 180 x L30	No	3
GISS-E2-R	NASA Goddard Institute for Space Studies	Atm: 144 x 90 x L40 Ocn: 288 x 180 x L32	No	3
IPSL-CM5A-LR	Institut Pierre Simon Laplace, France	Atm: 96 x 96 x L39 Ocn: 182 x 149 x L31	Yes	3
MIROC-ESM	Center for Climate System Research, JAMSTEC, Japan	Atm: 128 x 64 x L80 Ocn: 256 x 192 x L44	Yes	3
MPI-ESM-P	Max Planck Institute for Meteorology, Germany	Atm: 196 x 98 x L47 Ocn: 256 x 220 x L40	Yes	3
MRI-CGCM3	Meteorological Research Institute (MRI)	Atm: 320 x 160 x L48 Ocn: 364 x 368 x L51	No	3

https://doi.org/10.5194/cp-2019-58
Preprint. Discussion started: 13 June 2019

Table 2. List of experiments included in the CESM LGM and PI ensemble. The following abbreviations are used: noVeg = No interactive vegetation; Veg = Including interactive vegetation; PI = pre-industrial; LGM = Last Glacial Maximum; CAM4/5 = Community Atmosphere Model version 4 or version 5; GLAC-1D = GLAC-1D ice sheet reconstruction (Tarasov et al., 2012; Briggs et al., 2014); ice6g = ICE-6G ice sheet reconstruction (Peltier et al., 2015).

Ensemble	Experiment name	Atmospheric model	Interactive vegetation	Boundary conditions	LGM ice-sheet reconstruction
PI reference simulations	PI_CAM4_noVeg	CAM4	No	PI	
	PI_CAM5_noVeg	CAM5	No	PI	
	PI_CAM4_Veg	CAM4	Yes	PI	
	PI_CAM5_Veg	CAM5	Yes	PI	
Atmospheric model physics	LGM_CAM4_noVeg	CAM4	No	LGM	GLAC-1D
	LGM_CAM5_noVeg	CAM5	No	LGM	GLAC-1D
Interactive vegetation	LGM_CAM4_noVeg	CAM4	No	LGM	GLAC-1D
	LGM_CAM4_Veg	CAM4	Yes	LGM	GLAC-1D
	LGM_CAM5_noVeg	CAM5	No	LGM	GLAC-1D
	LGM_CAM5_Veg	CAM5	Yes	LGM	GLAC-1D
Continental ice sheets	LGM_CAM5_noVeg	CAM5	No	LGM	GLAC-1D
	LGM_CAM5_noVeg_ice6g	CAM5	No	LGM	ICE-6G